

Analysis of GRACE range-rate residuals with focus on KBR instrument system noise

Sujata Goswami^{1,*}, Balaji Devaraju¹, Jakob Flury¹

1 Institut für Erdmessung, Schneiderberg 50, 30167 Hannover

* goswami@ife.uni-hannover.de

Abstract

We investigate the range-rate residuals that come out of the gravity field parameter estimation, called the *post-fit residuals*, from the inter-satellite ranging data of the GRACE (Gravity Recovery and Climate Experiment) satellite mission. Particularly, we investigate the high-frequency spectrum of the post-fit residuals ($f > 20$ mHz). Such analysis is carried out to understand the yet unsolved discrepancy between the predicted baseline errors and the observed ones. Initially, we analyse the characteristics of the signal-to-noise ratios of the four frequencies of the GRACE microwave ranging system. The SNR of the ranging system contains signatures of sun and moon intrusions, temperature changes in the instrument and changes in the magnetic torquer rod currents. Subsequent analysis of the high-frequency range-rate residuals reveals that they are affected by all the effects, except magnetic torquer rod currents. In order to ascertain the impact of these systematic errors on the estimated parameters, we compare the post-fit residuals with the pre-fit residuals. This comparison shows that at least 30 % of the systematic effects end up in the parameters estimated during gravity field parameter estimation.

Introduction

Since 2002, GRACE mission has provided the time-variable measurements of the gravity field of the Earth by measuring the distance between the two satellites (range) flying in a low earth orbit [Tapley et al., 2004]. These range observations are the main observables that are used in the global gravity field determination. Due to their unprecedented accuracy (in μm) the recovery of the time-variable gravity and mass changes has been possible, which has enabled a vast number of applications in hydrology, cryology and climate studies. Although the accuracy of the time-variable gravity field measurements is unprecedented, still, there is an order of magnitude difference between the current accuracy of the GRACE solutions and the baseline accuracy that was predicted by Kim [2000] prior to its launch (cf. Fig. 1). The systematic errors from sensors, errors from the background models are known to be the reasons behind this limited accuracy achieved in the current gravity field solutions. However, it is important to fully understand the source of these errors which affects the accuracy of the gravity field solutions.

The range-rate residuals obtained after full parameter estimation chain contain these errors. Thus, an analysis of the GRACE range-rate residuals is important to understand the source of various systematic errors absorbed by them. The knowledge of those error sources is required also to understand the error budget of GRACE. A full understanding

of the systematic errors in the ranging data is necessary to improve the data pre-processing strategies, which is an important step for the global gravity field parameter estimation. Recent investigations of sensor data, for example, star camera [Bandikova & Flury, 2014, Ko et al., 2015] and accelerometer [Klinger & Mayer-Gürr, 2016], have improved their pre-processing strategies resulting in significant improvement in the quality of the estimated gravity field. These studies serve as good examples and a motivation for the analysis of the range-rate residuals.

The expected sensor noise level in the range-rate observations predominantly consists of the accelerometer, star camera noise and KBR instrument system noise. While the noise behaviour of the accelerometer and the KBR system noise are known and are described by models (cf. Fig. 1), the noise behaviour of the star camera, and hence its model, is not known. The power spectral density of range-rate residuals closely follow the accelerometer noise model in the low frequencies—noise decreases with increasing frequency, and in the higher frequencies it follows the KBR system noise model—noise increases with increasing frequency (cf. Fig. 1). In this study we will analyse the KBR system noise and identify the hitherto unknown systematic effects.

Earlier, the microwave ranging system was comprehensively studied by Thomas [1999] prior to the launch of GRACE, and it was demonstrated that the ranging system noise dominated the frequencies beyond 20 mHz, i.e., the *high frequencies* (cf. Fig. 1). Ko [2008] investigated the time-series of the high-frequency post-fit residuals and provided initial strategies for analysing sensor noise. This was followed by an analysis of the signal-to-noise ratio (SNR) of the ranging system [Ko et al., 2012], which correlated the poor SNR values of the ranging system with the high-frequency range-rate residuals. However, the study did not establish the source of the poor SNR values.

Goswami & Flury [2016] investigated the sources of the SNR variations, and attributed them to star camera intrusions and temperature variations in the sensor unit. It was found that the temperature variations in the sensor unit contributed most to the SNR variations and they ended up in the range-rate residuals. It was also speculated that the changes in magnetic torquer rod currents had an impact on the SNR and hence the range-rate residuals. Harvey et al. [2016] analysed the SNR data from 2006–2013 and identified that the thermistor located near the ranging system contributed to the temperature variations seen in the SNR. They also confirmed the impact of the sun intrusions into SNR.

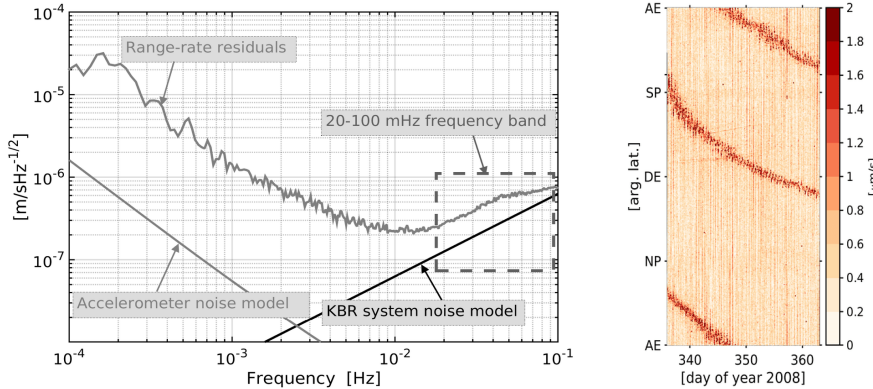


Figure 1. *Left:* Power spectral density of postfit range-rate residuals plotted for December 2008; *right:* post-fit range-rate residuals plotted along argument of latitude and time. Argument of latitude ranges from 0° to 360° starting from the bottom. Y-axis represent the AE - Equator pass during ascending orbit (0°), NP - North Pole (90°), DE - Equator pass during descending orbit (180°), SP - South Pole (270°). These plots are mostly used in rest of our analysis.

In this contribution, firstly, we extend the analysis of SNR to show the effects of moon intrusions into the SNR and to confirm the role of magnetic torquer rod currents. Secondly, we look at the high-frequency range-rate residuals to see for the signatures of the identified systematic effects. Finally, we ascertain whether the systematic effects, identified thus far, end up in the estimated parameters. We present an analysis for the two years of GRACE data that is 2007 and 2008.

1 GRACE K-band ranging (KBR) system and system noise

The microwave ranging system of GRACE, widely known as K-band ranging system (KBR), measures the dual one way K-band range change between the two satellites with the precision of $1 \mu\text{m/s}$. The KBR system consists of a single horn antenna for the transmission and reception of the dual band and K- (24 GHz) and Ka-band (32 GHz) microwave signals, an Ultra Stable Oscillator (USO), a Micro Wave Assembly (MWA), an Instrument Processing Unit (IPU), an accelerometer and Star Camera Assembly (SCA) carrying two star cameras. IPU is used for sampling and digital signal processing of the K-band carrier phase signals and the data of the GPS space receiver [Dunn et al., 2002, Flechtner, 2000].

The GRACE K-band ranging instrument transmits carrier phase signals modulated on two frequencies namely K- and Ka-band. Each spacecraft carries two carrier phase signals each, the biased range is computed from the combination of these four carrier phase observations as described in Thomas [1999]. This combination is done in KBR level 1A (L1A) to level 1B (L1B) processing [Wu & Kruizinga, 2008]. As the two frequencies are modulated on the carrier phase signals, these are highly affected by the phase (ϕ) errors.

The $1-\phi$ error corresponding to the SNR for 1 second-interval data is given, in units of cycles, as [Thomas, 1999]

$$\sigma_{\phi,A}^{K/Ka} = \frac{1}{2\pi(\text{SNR}_{K/Ka})} \quad (1)$$

The phase error of the K- and Ka-band frequencies of both the spacecrafts is computed from the $1-\phi$ error and it is given as

$$\begin{aligned} \sigma_{\phi}^K &= c \frac{\sqrt{(\sigma_{\phi,A}^K)^2 + (\sigma_{\phi,B}^K)^2}}{f_A^K + f_B^K} \\ \sigma_{\phi}^{Ka} &= c \frac{\sqrt{(\sigma_{\phi,A}^{Ka})^2 + (\sigma_{\phi,B}^{Ka})^2}}{f_A^{Ka} + f_B^{Ka}} \end{aligned} \quad (2)$$

where c is the speed of light and f_i^K and f_i^{Ka} are the nominal frequency of K- and Ka-band of GRACE-i, ($i \in \{A, B\}$).

The noise of the KBR microwave system is computed from the phase errors of K- and Ka-band frequencies as follows:

$$\sigma_{\phi} = \sqrt{\frac{[(f_e^K)^2 \sigma_{\phi}^K]^2 + [(f_e^{Ka})^2 \sigma_{\phi}^{Ka}]^2}{[(f_e^K)^2 - (f_e^{Ka})^2]^2}} \quad (3)$$

where f_e is the effective frequency and $\sigma_{\phi}^{K/Ka}$ is the phase error of K/Ka-band respectively. Thus, the KBR system noise is related to the SNR of all the transmitted

signals.

The KBR system noise σ_ϕ is highly dominated in the frequencies above 20 mHz. The KBR system noise is highly dominated by the phase errors of four frequencies (K- and Ka-band frequencies of each spacecraft) [Ko, 2008]. The phase error of each frequency is inversely proportional to the SNR of that frequency (cf. Eqn. 1). Thus, low SNR corresponds to the high phase errors which leads to the high system noise. The SNR is the amount of power in 20 ms integrations of signal power (integrated against a phase locked local model) compared to an integration with local model in quadrature. These SNR values reflect the measure of signal strength and ranging measurement quality.

The GRACE mission requirements for SNR values are greater than or equal to 630 (0.1 db-Hz) [Harvey et al., 2016]. These values are also used during L1A to L1B processing of KBR data done at JPL, NASA. The phase observations with SNR values > 450 are used to compute range and range-rate observations, observations below SNR 450 are removed. Due to the anomalous behavior of the Ka-band SNR of GRACE-B, they are not considered in filtering, during the processing of KBR data [Wu & Kruizinga, 2008].

In Fig. 2, the SNR time-series plotted for one day shows that the values except Ka-band SNR of GRACE-B, which are anomalous, are greater than 580. They show once-per-rev (K- and Ka-band SNR of GRACE-A) and twice-per-rev (K-band SNR of GRACE-B) periodicities. The drop in SNR values in these periodicities is rather large for the K-band as compared to the Ka-band. In Fig. 3, we can see that the SNR of both the

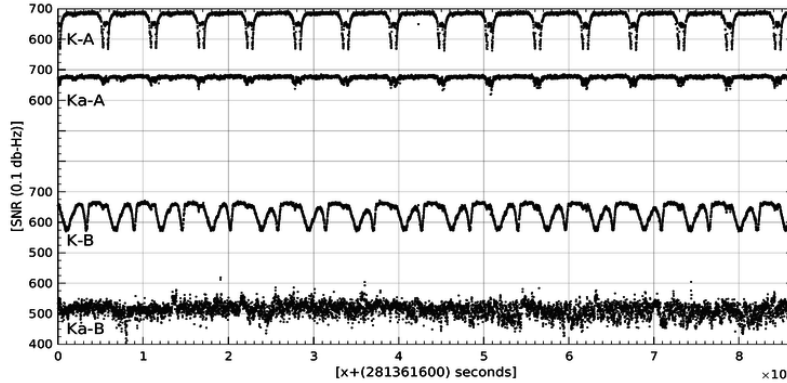


Figure 2. SNRs of four frequencies of GRACE-A and GRACE-B for the day December 1, 2008. Values are provided in the GRACE KBR1B data product.

frequencies of GRACE-A are correlated with each other except the fact that the drop in the K-band SNR values is stronger than that of the Ka-band SNR, which is similar to the behaviour seen in the time-series. The K-band SNR of GRACE-A and GRACE-B shows the same features, but GRACE-B shows some additional features and that they are far more prominent. The reasons behind these features, and the differences in their strengths are discussed in the following sections.

2 Star camera intrusion effects on SNR

The star camera is blinded by the intrusion of sun and moon, and they occur every 161 d and 27 d periods, respectively [Bandikova, 2015]. These effects are called *sun and moon intrusions*, which are one of the main contributors to the attitude errors. Both spacecrafts have two star cameras on board, designated as *head #1* and *head #2*. They are present on each of the lateral side of the spacecraft. Thus, most of the time only one

of the star camera heads is blinded by either sun or moon while other being available for the acquisition of the attitude. When anyone of the star camera head is blinded, the other is set as the primary star camera which is available for attitude acquisition. The periods when both star camera heads are available, and none of them are blinded due to either sun or moon, the attitude is obtained from the combination of data from both of the star camera heads.

In the L1B star camera data (SCA1B), data flags are provided when the star cameras were available and when not. Fig. 3 shows the sun and moon intrusions into the star camera of each satellite during the year 2007 and 2008. It is clear that due to the inline orbit formation of the GRACE satellites both the satellites go through sun and moon intrusions simultaneously, and also we see that the head that is available from each satellite during blinding periods is alternating – head #1 of GRACE-A and head #2 of GRACE-B are available and *vice versa*. The SNR values are also affected during the period when one of the star camera heads is blinded by the either sun or moon. Fig. 3 shows strong drops in the K-band SNR of GRACE-A when one of the star camera heads transits into the sun blinding phase and *vice versa*. When star camera is completely blinded by sun, the SNR comes back to normal (> 630). This leaves the ring like structure with depressed SNR surrounded by the regions of high SNR. The effect on the SNR could be due to the on board processing of the star camera data, which may produce electromagnetic interference with the K-band ranging system, because the on board instrument processing unit (IPU) is located near the Microwave Assembly (MWA) [Harvey et al., 2016].

The signature left by the sun intrusion could be a function of the star camera baffle structure [Harvey et al., 2016]. The three SNRs are not only affected by the sun intrusions but also are affected by the moon intrusions into the star camera. Fig. 3 shows the zoomed-in moon intrusions into the star camera and SNR of K-band frequency of GRACE-B corresponding to that time. The structure formed due to the drop in the SNRs during moon intrusion exhibits the structure similar to the sun intrusion. This indicates that the structure formed in SNR due to moon intrusion could also be a function of the star camera baffle structure.

As shown in the Fig. 3, the strength of the ring structure caused by sun and moon intrusions is dependent on the spacecraft and the microwave frequency. It is stronger in the K-band of GRACE-A whereas weaker in the Ka-band of GRACE-A and the K-band SNR of GRACE-B. The GRACE-A uses the redundant microwave assembly since the launch of the mission while GRACE-B uses the main microwave assembly. The differences between the two instruments could be the reason behind the differences in the strength of the K-band SNR of both spacecrafts [Harvey et al., 2016]. However, the reason behind why the rings in Ka-band SNR of GRACE-A are also weaker than K-band SNR of same spacecraft may be due to the differences in the two transmitting frequencies. The transmit frequency of K-band is 502.524 kHz and Ka-band is 670.032 kHz.

The patterns dominated in the K-band SNR of the GRACE-B after day 200 in Fig. 3 are due to the temperature variations in one of the thermistors located near the KBR microwave assembly [Harvey et al., 2016].

3 Magnetic torquer rod current effects on SNR

In GRACE, there are three magnetic torquer rods on each spacecraft. They are used to maintain inter-satellite pointing within their limits (see Bandikova [2015] for details). The magnitude of the currents flowing through the rods depend upon the strength of magnetic force acting on the satellite. The effects of the magnetic torquer rod induced signals on the accelerometer has been studied earlier by Peterseim et al. [2012].

In Fig. 4, the absolute value of magnetic torquer currents of both satellites are

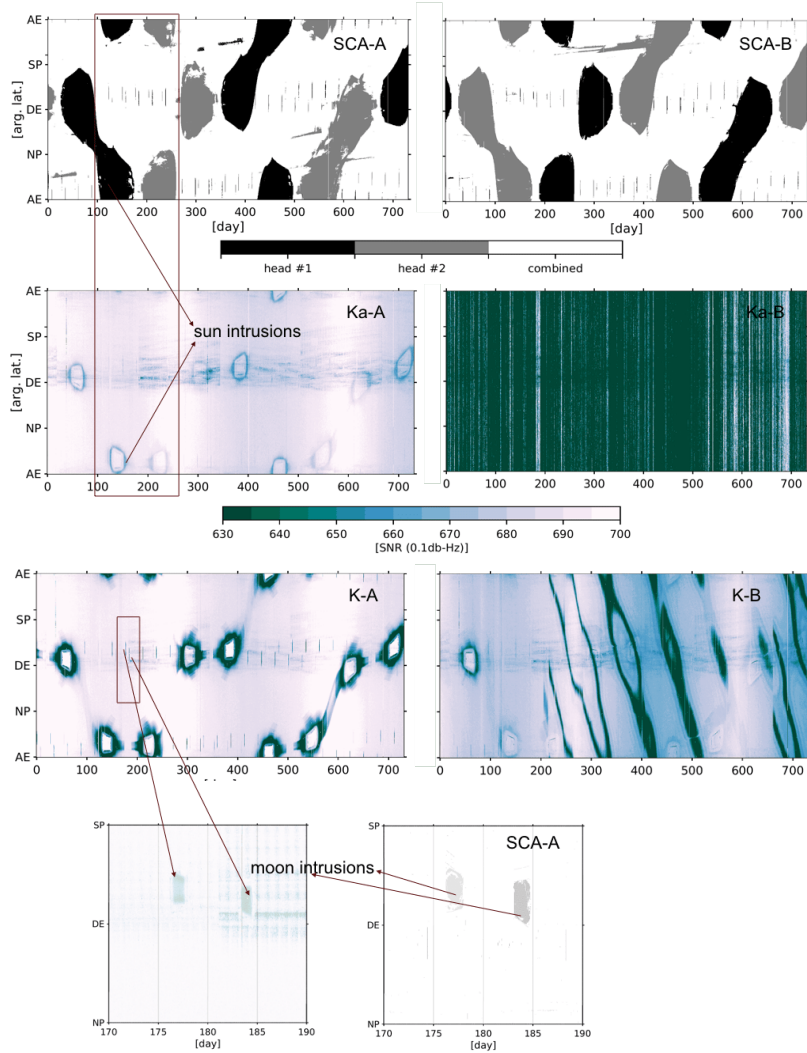


Figure 3. Star camera data flags of GRACE-A and GRACE-B are plotted for the year 2007 and 2008 in the 1st row. The colorbar indicates the color representing when one of the two heads were blinded and when both were heads were available. Black color represents the time-period when *head#1* was blinded in both satellites, gray color presents when *head#2* was blinded and the white color represents when none of the star camera heads were blinded. 2nd row shows the Ka-band SNR of GRACE-A and GRACE-B; 3rd row shows the K-band SNR of both satellites. Last row shows the zoomed-in picture of moon intrusions into the SNR of K-band SNR of GRACE-A and their correlation with the moon intrusions into the star camera of the corresponding spacecraft.

plotted along the argument of latitude for the two year period i.e. 2007 and 2008. The 161 d periods of high currents are clearly visible in all the three torquer rod currents of two spacecraft. During year 2007 and 2008, the good star camera on both spacecrafts was head#2 and bad star camera was head#1. When the head#2 was set as the primary star camera, the currents in the magnetic torquer rods were smooth whereas the currents were comparably high when head#1 was set as the primary star camera for attitude acquisition (Personal Comm. Tamara Bandikova). Considering GRACE-A in Fig. 4, the torquer rod currents were high in all the three rods when the bad star camera head was active and good star camera head was sun or moon blinded (see Fig. 3). It is vice-versa in GRACE-B.

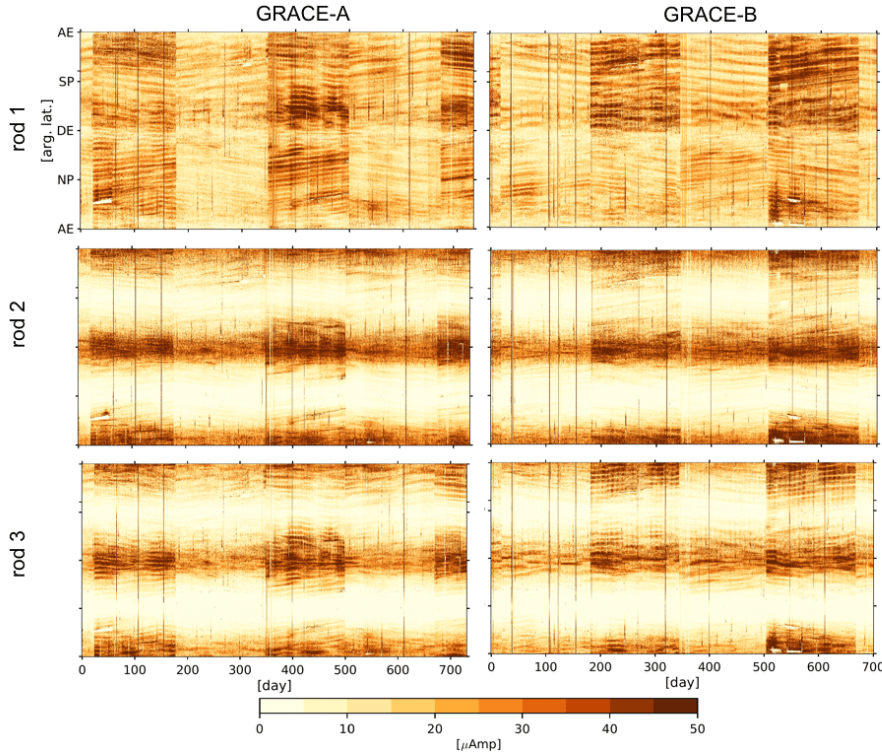


Figure 4. Absolute value of currents in the three magnetic torquer rods of GRACE-A and GRACE-B for 2007 and 2008. Periods of 161 days with high currents along the equator (descending and ascending) can also be seen which are related to satellite attitude.

The SNRs of the K- and Ka-band of the GRACE-A and K-band of GRACE-B seems to be affected by the currents flowing through the magnetic torquer rods of GRACE-B. The correlation of the SNRs is high with the currents flowing through the magnetic torquer rod 3 of the GRACE-B. Fig. 5 shows the torquer rod current dependent effects in all the three SNRs which were affected due to the torquer rod currents of GRACE-B only. No variation due to GRACE-A has been seen. The currents flowing through the magnetic torquer rod 3 of GRACE-B has been plotted for the 250 days of 2007. The smooth currents were flowing the rod from day 19 to 180 as the primary star camera during this time was head#2. The strong currents flowing through the rods from the days 1 to 19 and from 181 until 250 due to bad star camera head#1. The period when currents were strong in the magnetic torquer rod 3, all the three SNRs were affected and show similar variations. The region with strong currents are also highlighted in the Fig. 5. Although the SNRs were affected due to the magnetic torquer rod currents still, none of the three SNRs dropped below mission requirements (>630).

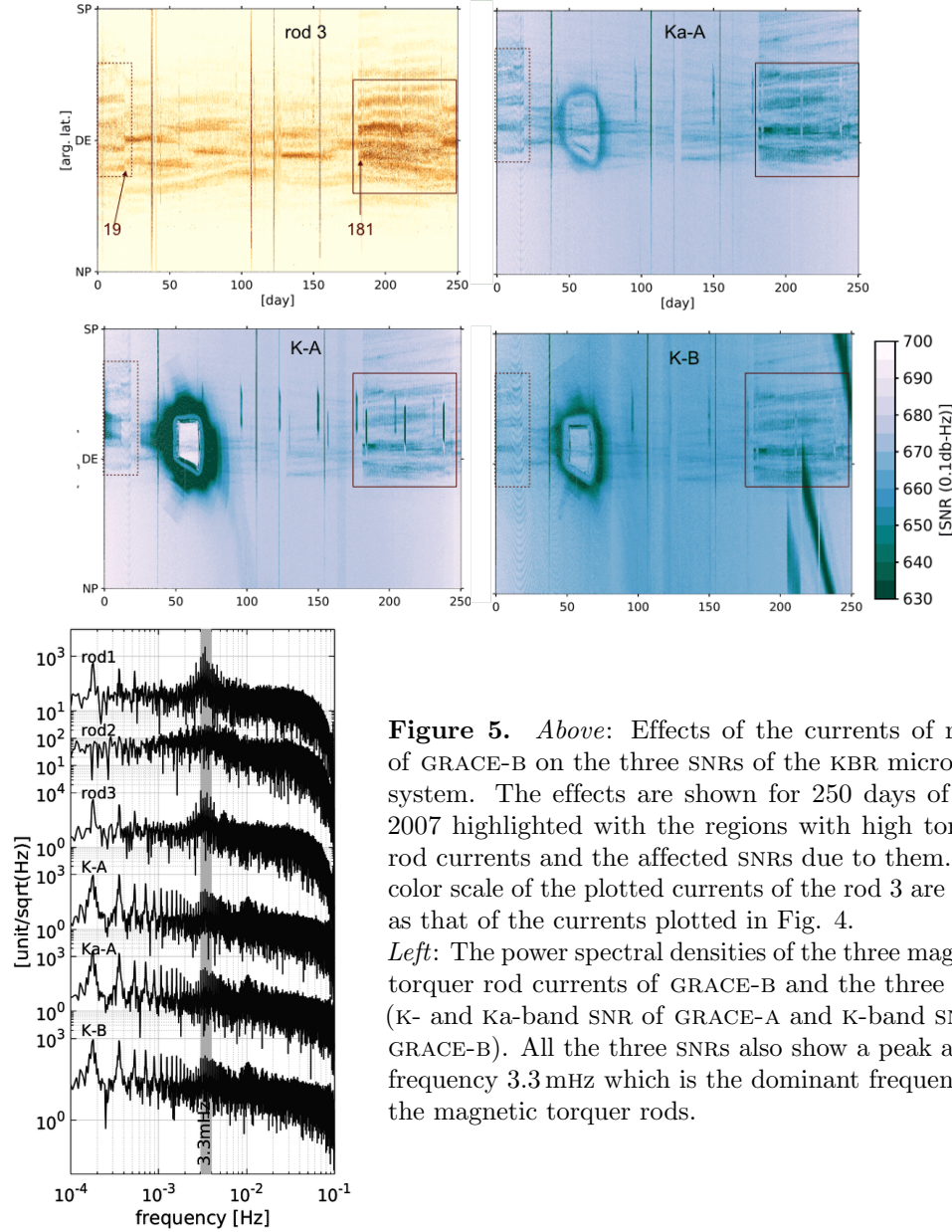


Figure 5. *Above:* Effects of the currents of rod 3 of GRACE-B on the three SNRs of the KBR microwave system. The effects are shown for 250 days of year 2007 highlighted with the regions with high torquer rod currents and the affected SNRs due to them. The color scale of the plotted currents of the rod 3 are same as that of the currents plotted in Fig. 4.

Left: The power spectral densities of the three magnetic torquer rod currents of GRACE-B and the three SNRs (K- and Ka-band SNR of GRACE-A and K-band SNR of GRACE-B). All the three SNRs also show a peak at the frequency 3.3 mHz which is the dominant frequency of the magnetic torquer rods.

The power spectral densities of the three SNRs show the signatures of the frequency corresponding to the rod currents of GRACE-B (cf. Fig. 5). The frequency 3.3 mHz is associated with the pointing variations between the two GRACE spacecrafts [Bandikova et al., 2012].

4 Analysis of GRACE post-fit range-rate residuals

As discussed in previous sections the SNR of all four frequencies exhibit different behavior which are dependent on the intrusions, high magnetic torquer currents and instrument temperature variations. From Eqn. 2, the KBR system noise is directly proportional to the phase error of the nominal frequencies. This noise is dominated in

frequencies above 20 mHz [Ko, 2008, Thomas, 1999]. Here, we analyze the post-fit residuals in order to understand the system noise dependent errors present in them. The post-fit residuals are computed using the standard ITSG-2014 global gravity field parameter estimation chain (see A for details). The computed post-fit residuals are plotted along the argument of latitude and time for the two year duration starting from 1 January 2007 in Fig 6. These post-fit range-rate residuals are analysed in following sections.

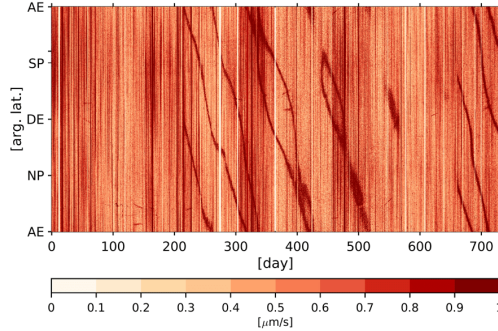


Figure 6. Postfit range-rate residuals computed using the ITSG-2014 parameter estimation chain. The residuals are plotted for the two year duration starting from 1 January 2007.

4.1 Noise characteristics of the high frequency post-fit range-rate residuals

This section focuses on the understanding of the characteristics of the noise in the high frequency post-fit range-rate residuals (>20 mHz). An understanding of the noise characteristics in these frequencies is important for the identification of different source of errors in the range-rate observations. As seen in Fig. 6 one of the most interesting feature in the post-fit range-rate residuals is the pattern of bands with high value of postfits which begins from day 200 and continues until the end of December 2008 (day 730). The structure of these bands changes and repeats after a shift in time. The high noise forming these bands like pattern is related to the temperature dependent variations in the SNR of GRACE-B which is dominated in the postfits.

The postfits are filtered using highpass and lowpass filter to filter frequencies above and below 20 mHz respectively (The LTPDA toolbox is used here for filtering the postfits Hewitson [2007]). The high pass filtered residual vector is denoted as (\hat{e}_{HP}) and the low pass filtered residual vector is denoted as (\hat{e}_{LP}) . The temperature dependent noise in the K-band SNR of GRACE-B (cf. Fig. 3) is dominating in the frequencies above 20 mHz as shown in Fig. 7. There are also regions where the postfits are slightly high.

The high amplitude of postfits seems to be correlated with the SNR suffering from the sun intrusions. The amplitude of the residuals is high where the K-band SNR of GRACE-A drops in the inner ring structure caused by the sun intrusions as shown in Fig. 7 as a zoomed-in plot. However, the signatures are not as strong as temperature dependent errors in postfits. This could be due to the periodic nature of the sun intrusion dependent effects in the SNRs with a repeat period of 161 days (also once-per-rev). Due to their periodicity the intrusion related errors in the range-rate observations are more likely to be absorbed by the estimated parameters as compared to the temperature dependent errors which are non-periodic in nature. Therefore, the strength of patterns related to them are weaker than the temperature related errors.

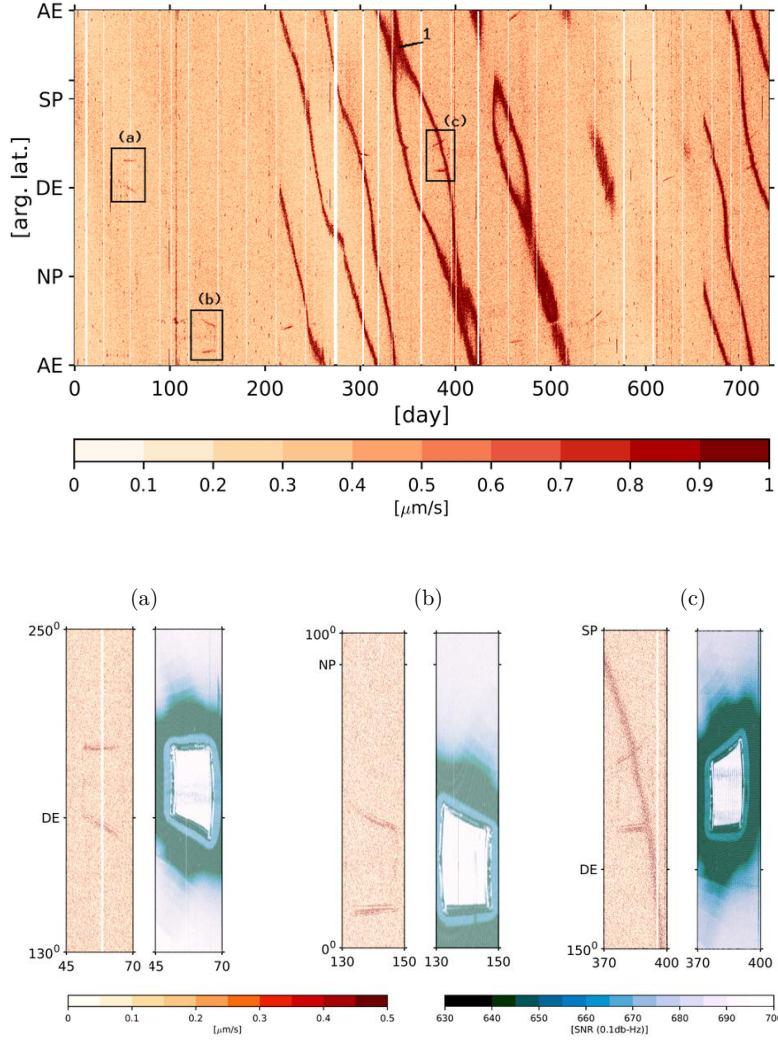


Figure 7. *Above:* High frequency postfit residuals (\hat{e}_{HP}) plotted for year 2007 and 2008 along the argument of latitude and time in days; temperature dependent bands are marked as ‘1’ and ‘(a)’, ‘(b)’, ‘(c)’ are the effects related to the sun intrusions; *below* are the zoomed-in picture of the residuals correlated with the sun intrusions related effects in the SNRs. The K-band SNR of GRACE-A is plotted here to show the correlation with postfits.

4.2 Contribution of high-frequency noise to the post-fit range-rate residuals

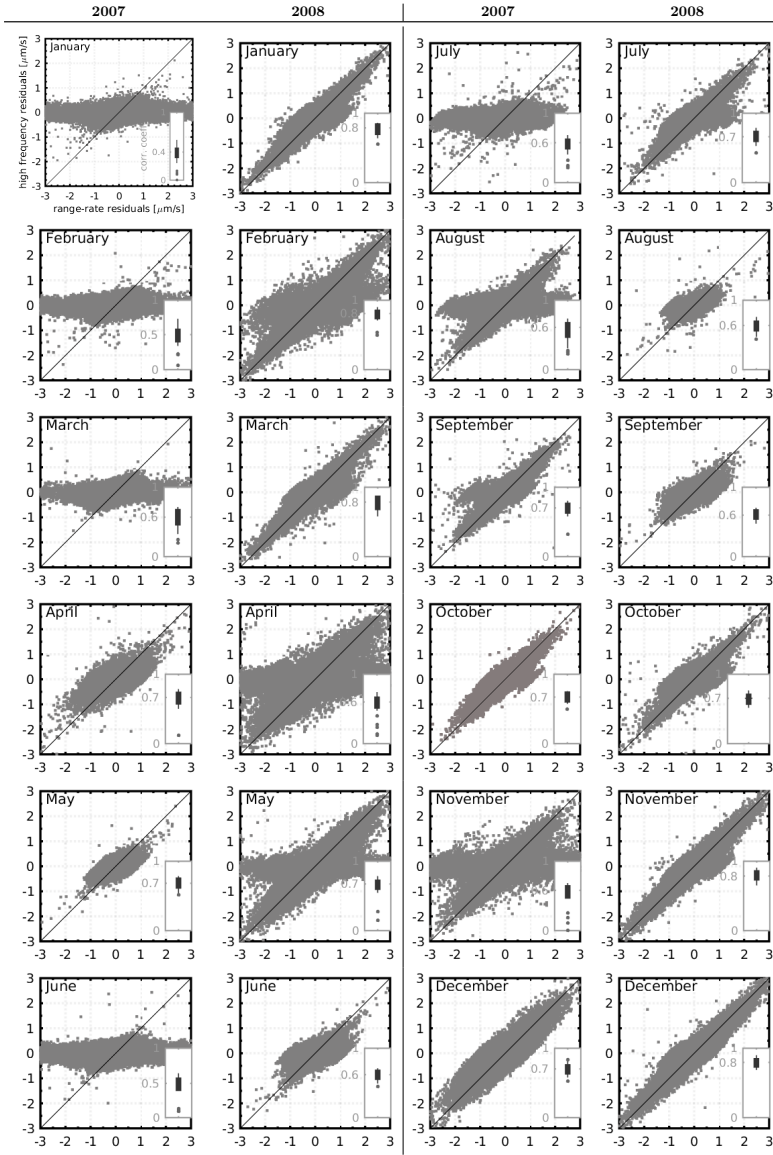


Figure 8. Monthly scatter plots between the vector \hat{e} (x-axis) and (\hat{e}_{HP}) (y-axis) show the correlation between them. Correlation coefficients between the two vectors are plotted as box plot. Coefficients are computed once per day for each month.

The noise dominated in the post-fit residuals is dependent on time and SNR variations, which make it inhomogeneous in nature. Monthly scatter plots are used to describe their variations over a period of month (cf. Fig. 8). Due to the inhomogeneous nature of noise in the post-fit residuals, the correlation coefficients are computed once per day and are shown in the box plots plotted along with the scatter plots. The correlation coefficient should explain the percentage of high frequency noise (\hat{e}_{HP}) present in the full residual vector. The months where the temperature dependent noise in the SNR of K-band of GRACE-B was dominating (for example, January 2008), the

correlation of high frequency noise (\hat{e}_{HP}) is very high with the post-fit residuals (\hat{e}). In January 2007, the temperature related noise was not present in the observations therefore the correlation of postfits with the high frequency noise is very small. However, there are certain months where the high correlation does not seem to be dependent on the SNRs noise for example April and May 2007. The high correlation between (\hat{e}) and (\hat{e}_{HP}) for these months could be due to the error sources other than the SNR noise which is still unknown.

4.3 Comparison of the noise in post-fit residuals with the noise in pre-fit residuals

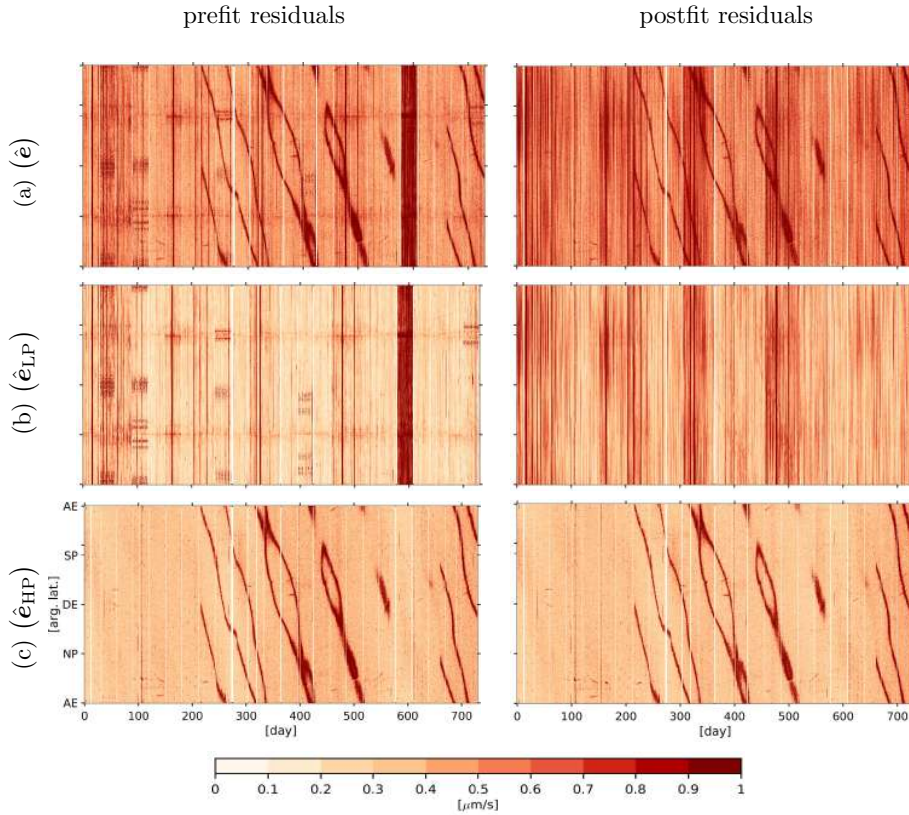


Figure 9. Comparison of pre-fit and post-fit residuals (a) and their lowpass (b) and highpass filtered parts (c). The darkest patch from the day 578 to 609 shows that the prefits were comparatively higher for the month of August 2008 than the other months. However, the solution converged with the noise level comparable to other months as can be seen in the postfits.

In order to investigate whether the high frequency noise is propagated into the estimated parameters, in this section, we take differences between the pre-fit and the post-fit residuals. Here, the estimated parameters include unknown initial positions of the orbit determination problem, scale and bias of the accelerometer and gravity field coefficients. In general, the pre-fit residuals must have more signal than the post-fit residuals, and hence their differences must be positive. Further, the difference should indicate the signal that has been absorbed by the estimated parameters. Since the KBR noise is observed in the high-frequency part, we look at the difference between the full

signals, their low-frequency (<20 mHz) parts as well as the high-frequency parts (>20 mHz).

The differences between the pre-fit residuals and post-fit residuals (cf. Fig. 9) show that the contribution of low frequencies into the estimated parameters is significantly high than the high frequencies. They are highly correlated with the differences of the lowpass filtered parts of the post-fit and pre-fit residuals. The noise in the low frequencies (<20 mHz) is dominated by the attitude errors, accelerometer dependent errors and errors from geophysical models which are reduced from the range-rate observations during gravity field parameter estimation (cf. Fig. 9). The analysis of this low frequency noise is beyond the scope of this paper. However, the minimal contributions from the high frequency noise cannot be neglected.

The differences of the high frequency filtered set of residuals plotted on the different color scale shows the amount of noise which might be going into the estimated parameters. The contribution of the high frequency noise could go up to 30 % of the total noise contribution. Again, it should be kept in mind that this 30 % could be distributed in any of the above mentioned estimated parameters.

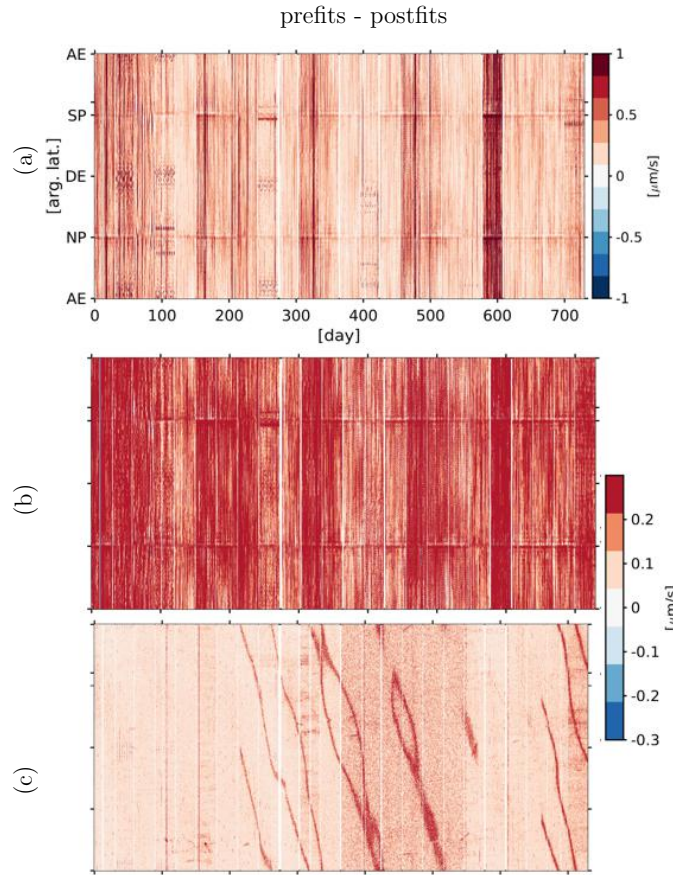


Figure 10. Differences between the pre-fit and post-fit residuals. (a) shows the differences between the full residual (\hat{e}) vectors, (b) shows the lowpass filtered part of the differences between the prefits and postfits and (c) presents the highpass filtered part of the corresponding differences.

5 Summary and Discussions

We have shown that the SNRs are highly affected by the GRACE Attitude and Orbit Control System (AOCS). The intrusions into the star camera not only limits the accuracy of the GRACE attitude but also affects the SNRs of the three frequencies of the spacecraft. The temperature related problems were limited to just one of the three SNRs (that is, the K-band SNR of GRACE-B) but the star camera blinding affected all the three SNRs (cf. Fig. 3). However, the impact on the performance of each SNR due to these effects was different but can not be neglected.

The K-band SNR of GRACE-A dropped below the mission requirements due to the sun and moon intrusions. This clearly shows that the attitude affecting SNR is not good for the performance of the mission. The effects of the magnetic torquer rod currents of GRACE-B on the SNRs were not large but cannot be neglected (cf. Sec. 3). Overall, the impact of the attitude variations on the SNRs of the frequencies of K-band microwave ranging system of GRACE can not be ignored. The improvements are required to be done on this side.

The impact of the instrument temperature variations on one of the key components (that is, the microwave assembly) could be a limiting factor of the mission performance (cf. K-B in Fig. 3 and [Goswami & Flury, 2016, Harvey et al., 2016] for details). This could have been better in absence of these effects. The temperature variations would have affected the performance of the future geodesy missions too, such as GRACE-Follow On (GFO). Thanks to the continuous efforts ongoing to analyze the GRACE data, the errors in the ranging data due to the temperature variations affecting its main sensors has been detected while the GFO is still on-ground [Bandikova et al., 2012, Goswami & Flury, 2016, Harvey, 2016, Harvey et al., 2016, Klinger & Mayer-Gürr, 2016]. These sensors will be shielded now to protect them from the internal temperature variations especially the KBR microwave assembly (Personal comm. Gerhard Kruizinga). So, this would not be a problem in the GRACE-Follow On (GFO).

On the other hand, it is possible that the effects related to intrusions and magnetic torquer currents would still effect the SNRs of the GRACE-Follow On. This is due to the similarity in the construction of the two satellites. Also, until now it is assumed that the intrusions into the SNR are not a problem [Harvey et al., 2016] as they have not been seen in the post-fit residuals before. As we show that there are slight signatures related to the sun intrusions in to the SNR end up in the post-fit residuals. Their periodic nature which is once-per-rev (161 day period full cycle) makes it more easy to be absorbed by the estimated parameters. Due to their similar periodic behavior it is likely that these errors might alias with the S2 tide. This could also be the reason why we do not see the strong patterns related to the sun intrusions as we see the patterns related to the temperature variations in the post-fit residuals.

Acknowledgements

This project is funded by DFG as SFB 1128 geo-Q. We would like to thank Matthias Weigelt, Beate Klinger, Torsten Mayer-Gürr for helpful and detailed discussions.

A Gravity field parameter estimation

The standard GRACE KBR1B product provided by the JPL, NASA is used to compute the global gravity field solution. The product contains range-rate observations with 5s sampling interval along with light-time corrections and antenna center offset corrections which are added to range-rate observations. The global gravity field parameters are computed using ITSG-2014 processing standards [Mayer-Gürr, 2014]. The ITSG-2014 solution is computed using the variational equations approach up to degree and order 60. Details regarding data processing and additional parameter estimation are provided in Mayer-Gürr [2014, 2015]. The modeling approach is shown in Fig. 11. The range-rate

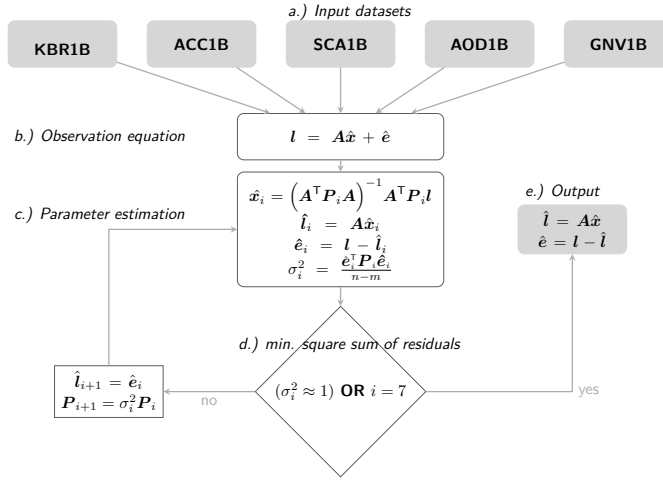


Figure 11. A forward modeling approach to model GRACE Level 1B data. In figure, P_i is the weight matrix at i^{th} iteration, σ^2 is the variance factor, n is the number of observations and m is the number of parameters.

observations vector used in our analysis (l) is obtained after reducing all the time-variable gravity field models (see, table 1) from the given range-rate observations. The design matrix is represented as A , \hat{x} contains the parameters to be estimated, \hat{e} is the vector of the range-rate residuals.

Acknowledgments

The project is funded by DFG as SFB 1128 geo-Q.

Table 1. Time-variable background models which are reduced from the range-rate observations during gravity field processing.

Models	Standards
Earth rotation	IERS 2003
Moon, sun and planet ephemeris	JPL DE421
Earth tide	IERS 2010
Ocean tide	EOT11a
Pole tide	IERS 2010
Ocean pole tide	Desai 2003 (IERS 2010)
Atmospheric tides (S1, S2)	Bode, Biancle 2003
Atmosphere and Ocean Dealiasing	AOD1B RL05
Relativistic corrections	IERS 2010
Permanent tidal deformation	includes (zero tide)

References

- Bandikova T., Flury J. & Ko U.D. 2012, Characteristics and accuracies of the GRACE inter-satellite pointing, *Advances in Space Research*, 50:123-135, doi: 10.1016/j.asr.2012.03.011
- Bandikova, T. & Flury, J. 2014, Improvement of the GRACE star tracker data based on the revision of the combination method, *Advances in Space Research*, 54(9): 1818-1827, doi: 10.1016/j.asr.2014.07.004
- Bandikova T. 2015, Role of attitude determination for inter-satellite pointing, Phd thesis, Leibniz Universität Hannover, Germany
- Dunn C., Bertiger W. & Franklin G. 2002, The Instrument on NASA's GRACE Mission: Augmentation of GPS to Achieve Unprecedented Gravity Field Measurements, *Proc. of the 15th Int. Tech. Meet. of Satellite Div. of The Ins. of Nav.*, 24 - 27 September 2002, Portland
- Flechtner F. 2000, GRACE Payload, <http://op.gfz-potsdam.de/grace/payload/payload.html>
- Goswami S. & Flury J. 2016, Identification and separation of GRACE sensor errors in range-rate residuals, GRACE Science Team Meeting, Potsdam, Germany
- Harvey N. 2016, GRACE star camera noise, *Advances in Space Research*, Vol. 58, No. 3, pp. 408-414 doi: 10.1016/j.asr.2016.04.025
- Harvey N., Dunn C., Kruizinga G. & Young L. 2016, Triggering Conditions for GRACE Ranging Measurement Signal-to-Noise Ratio Dips, *Journal of Spacecraft and Rockets*, Vol. 54, No. 1 (2017), pp. 327-330 doi: 10.2514/1.A33578
- Hewitson M. 2007, LTPDA, a MATLAB toolbox for accountable and reproducible data analysis, Max-Planck-Institut für Gravitationsphysik, Leibniz Universität Hannover Germany, https://www.elisascience.org/ltpda/usermanual/ug/sigproc_iir.html
- Kelley C., Kruizinga G. & Wu S.C. 2010, GRACE Level 1B Data Product User Handbook

-
- Kim J. 2000, Simulation Study of A Low-Low Satellite-to-Satellite Tracking Mission, Phd thesis, Center for Space and Research, Texas, US
- Klinger B. & Mayer-Gürr T. 2016, The role of accelerometer data calibration within GRACE gravity field recovery: Results from ITSG-2016, Adv. in Space Res., Vol. 58, 1597-1609, doi: 10.1016/j.asr.2016.08.007
- Ko U.D. 2008, Analysis of the characteristics of the GRACE dual one way ranging system, Phd thesis, Center for Space and Research, Texas, US
- Ko U.D., Tapley B., Ries J.C. & Bettadpur S. 2012, High-Frequency Noise in the Gravity Recovery and Climate Experiment Intersatellite Ranging System, Journal of Spacecraft and Rockets, Vol. 25, No. 6 (2012), pp. 1163-1173, doi: <https://arc.aiaa.org/doi/pdf/10.2514/1.A32141>
- Ko U.D., Wang F. & Eanes J.R. 2015, Improvement of Earth Gravity Field Maps after Pre-processing Upgrade of the GRACE Satellite's Star Trackers, The Korean Society of Remote Sensing, Vol. 31, No. 4, pp.353-360, doi: 10.7780/kjrs.2015.31.4.8
- Mayer-Gürr T., Klinger B., Zehentner N. & Kvas A. 2014, ITSG-GRACE 2014, Oct., GRACE Science Team Meeting, Potsdam
- Mayer-Gürr T. 2015, Insights in the deterministic and stochastic modeling of the GRACE observations, Oct., Autumn School "Global Gravity Field Modeling from SST Data", Bad Honnef, Bonn, Germany
- Peterseim N., Flury J. & Schlicht A. 2012, Magnetic torquer induced disturbing signals within GRACE accelerometer data, Advances in Space Research, Vol. 49, pp. 1388-1394, doi: 10.1016/j.asr.2012.02.013
- Tapley B.D., Bettadpur S., Watkins M. & Reigber C. 2004, The gravity recovery and climate experiment: Mission overview and early results, Geophys. Res. Lett., Vol.31, L09607, doi: 10.1029/2004GL019920
- Thomas J.B. 1999, An analysis of Gravity-field estimation based on inter-satellite dual-1-way biased ranging, JPL Publication 98-15
- Wu S.C., Kruizinga G. & Bertiger W. 2008, Algorithm Theoretical Basis Document for GRACE Level-1B Data Processing V1.2, JPL, NASA